PREDICTION OF ATMOSPHERIC MTF AND
APPLICATION TO IMAGE RESTORATION,
BASED ON METEOROLOGICAL DATA

4th Quarterly Report

(Sept. 1994)
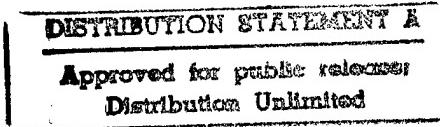
N. S. Kopeika, Principal Investigator

Department of Electrical and Computer Engineering

Ben-Gurion University of the Negev

Beer-Sheva, Israel

19980501 175

REPORT DOCUMENTATION PAGE

Form Approved OMB No. 0704-0188

Public reporting burden for this collection of information is estimated to average 1 hour per response, including the time for reviewing instructions, searching existing data sources, gathering and maintaining the data needed, and completing and reviewing the collection of information. Send comments regarding this burden estimate or any other aspect of this collection of information, including suggestions for reducing this burden to Washington Headquarters Services, Directorate for Information Operations and Reports, 1215 Jefferson Davis Highway, Suite 1204, Arlington, VA 22202-4302, and to the Office of Management and Budget, Paperwork Reduction Project (0704-0188), Washington, DC 20503.

1. AGENCY USE ONLY (Leave blank)	2. REPORT DATE September 1994	3. REPORT TYPE AND DATES COVERED Final Report

4. TITLE AND SUBTITLE

Prediction of Atmospheric MTF and Application to Image Restoration, Based on Meteorological Data.
4th Quarterly Report

5. FUNDING NUMBERS

F6170893W0896

6. AUTHOR(S)

I. Dror and N.S. Kopeika

7. PERFORMING ORGANIZATION NAME(S) AND ADDRESS(ES)

Ben Gurion University of the Negev
Department of Electrical and Computer Engineering
Beer Sheva, Israel 84105

8. PERFORMING ORGANIZATION REPORT NUMBER

SPC-93-40603

9. SPONSORING/MONITORING AGENCY NAME(S) AND ADDRESS(ES)

EOARD
PSC 802 BOX 14
FPO 09499-0200

10. SPONSORING/MONITORING AGENCY REPORT NUMBER

SPC-93-4060

11. SUPPLEMENTARY NOTES

12a. DISTRIBUTION/AVAILABILITY STATEMENT

Approved for public release; distribution is unlimited.

12b. DISTRIBUTION CODE

A

13. ABSTRACT (Maximum 200 words)

Predictions of atmospheric transmittance in desert aerosol environments using MODTRAN code diverge significantly from measured data. Good prediction of the desert particulate size distribution is required in order to predict atmospheric scattering and absorption parameters. It is also essential to the prediction of the aerosol atmospheric modulation transfer function which is often the dominant component of the overall atmospheric MTF. Recently an effort to predict statistics but not size distribution according to simple weather parameters has been made for coarse desert aerosols. A quantitative analysis of the desert particulate size distribution models was also performed. In this research, the size distribution parameters measured by optical counters are related to weather parameters. Known statistical and analytical models such as MODTRAN relate the size distribution parameters only to relative humidity for continental atmospheres. Although humidity has a significant role in the prediction of aerosol size statistics, other weather parameters are seen here to strongly influence also the size distribution parameters. Comparisons such as the above can be used to predict under which conditions the MODTRAN aerosol models have good or poor accuracy. It is also hoped that they will lead to improvements in MODTRAN, improving the accuracy of the humidity dependence as well as by incorporating other meteorological parameters into the MODTRAN prediction models.

DTIC QUALITY INSPECTED 5

14. SUBJECT TERMS

15. NUMBER OF PAGES

16. PRICE CODE

17. SECURITY CLASSIFICATION OF REPORT	18. SECURITY CLASSIFICATION OF THIS PAGE	19. SECURITY CLASSIFICATION OF ABSTRACT	20. LIMITATION OF ABSTRACT
UNCLASSIFIED	UNCLASSIFIED	UNCLASSIFIED	UL

NSN 7540-01-280-5500

Standard Form 298 (Rev. 2-89)
Prescribed by ANSI Std. 239-18
298-102

PREDICTION OF ATMOSPHERIC MTF AND APPLICATION TO IMAGE RESTORATION, BASED ON METEOROLOGICAL DATA

Fourth Quarterly Report

The Third Quarterly Report contained a statistical model for predicting size distribution of coarse aerosols (radius > 0.16 μm) according to weather forecast. This applies to arid or semi-arid regions in which the soil is dry so that soil-derived particulates are uplifted by the wind. The smaller fine particulates are then modelled with MODTRAN or LOWTRAN 7.

A detailed comparison of aerosol MTF prediction with aerosol MTF measurement indicates the reliability of this model is excellent, except for extreme cases defined in The Third Quarterly Report in which the aerosol size distribution model does not hold. Unfortunately, quantitative results of this comparison of MTF prediction with measurement are not yet complete. Qualitatively, they indicate the coarse aerosol size distribution prediction is excellent.

Here, a statistical model for predicting coarse aerosol size distribution according to weather for areas in which soil moisture prevents much uplifting of soil-derived particulates is presented in Appendix 1. This pertains to climates which are not arid or semi-arid.

Appendix 2 contains a step-by-step procedure to calculate aerosol MTF, based on predicted aerosol size distribution (n(x) in step 10) and hardware field-of-view and dynamic range.[1] Step 12 in it can be used to predict atmospheric transmission τ_a according to weather ,where

$$\tau_a = \exp[- \int_0^L \sigma[\lambda, n(x), z']dz'. \tag{1}$$

In (1), σ is medium extinction coefficient calculated in step 12, and L is path length. Thus, the aerosol size distribution models for arid and non-arid regions can be used in

Apependix 2 to predict both aerosol MTF and atmospheric transmission according to meteorological coditions.

Finally, the image restoration work has continued, and a comparison of various techniques with which to restore images degraded by atmospheric blur is enclosed as Appendix 3. These techniques apply to visible and thermal infrared wavelengths, and are based upon predicted or measured atmospheric MTF. The improved Wiener filter presented in The First Quarterly Report yields best results when turbulence blur is significant. When aerosol blur is more dominant, a variety of techniques all yield similar results. In all cases, the inclusion of aerosol blur in the atmospheric MTF yield restoration limited by hardware alone, as if there were no atmospheric blur.

Reference

1.   D. Sadot and N. S. Kopeika, "Imaging through the atmosphere: practical instrumentation-based theory and verification of aerosol MTF," *J. Opt. Soc. Amer. A*, vol. 10, pp. 172-179, Jan. 1993.

Appendix 1

Statistical model for aerosol size distribution parameters according to weather parameters

I. Dror and N. S. Kopeika

Ben Gurion University of the Negev
Department of Electrical and Computer Engineering
Beer Sheva, Israel 84105

ABSTRACT

Predictions of atmospheric transmittance in desert aerosol environments using MODTRAN code diverge significantly from measured data. Good prediction of the desert particulate size distribution is required in order to predict atmospheric scattering and absorption parameters. It is also essential to the prediction of the aerosol atmospheric modulation transfer function which is often the dominant component of the overall atmospheric MTF.[1] Recently[2] an effort to predict statistics but not size distribution according to simple weather parameters has been made for coarse desert aerosols. A quantitative analysis of the desert particulate size distribution models was also performed[3]. In this research the size distribution parameters measured by optical counters are related to weather parameters. Known statistical and analytical models such as MODTRAN relate the size distribution parameters only to relative humidity for continental atmospheres. Although humidity has a significant role in the prediction of aerosol size statistics, other weather parameters are seen here to strongly influence also the size distribution parameters.

Comparisons such as the above can be used to predict under which conditions the MODTRAN aerosol models have good or poor accuracy. It is also hoped that they will lead to improvements in MODTRAN, improving the accuracy of the humidity dependence as well as by incorporating other meteorological parameters into the MODTRAN prediction models.

1. Introduction

The aerosols that are suspended in the atmosphere are a major factor that influence the quality of images that are propagating through the atmosphere. Scattering and absorption of light rays by the suspended aerosols contribute to the loss of contrast of the received image, forward light scattering in the direction of the image propagation also reduce the atmospheric modulation transfer function (MTF) and cause to image blur.

Prediction of the aerosol size distribution can lead to the prediction of the scattering and absorption coefficients and also the scattering phase function of the atmospheric propagating medium. These properties characterize the extinction coefficient of the atmosphere as well as the MTF of the atmosphere.

2. Experiment

The particulate size distribution of the atmosphere was measured over the radius range of 0.16 to 10 μm using a PMS CSASP-100 optical particles counter. The optical counter was located at a height of 25 m above ground. Integration time of half an hour was chosen and every half an hour the average particulate size distribution was recorded. Meteorological parameters were also measured close to the PMS location and the half hour average of the temperature, relative humidity, wind speed, wind direction and solar flux were also recorded. The measurements were taken at the Ben-Gurion University of the Negev in Beer-Sheva, Israel. Data was collected form June 1991. Both PMS counter and Campbell Scientific meteorological station were connected to a personal computer.

Since this research is trying to relate the aerosol particulate size distribution parameters to simple weather parameters, the integration time selected for counting and classifying particles according to their size was to be shorter than the meteorological time constants. On the other hand, a short integration time leads to a particulate size distribution curve with insufficient data which is hard to fit to a known size distribution model. In our measurements an integration time of half an hour was chosen as a compromise between the need for a smooth size distribution curve and the need to measure the aerosol statistics under stationary meteorological conditions.

Fig. 1. describes the changes in the standard deviation of the temperature during a typical summer day. The standard deviation here is calculated for measurement time periods of half an hour. Fig. 2 shows the changes in the standard deviation of the relative humidity during the same day. These figures show that the most rapid changes occur after sunrise and sunset. In our measurements the standard deviation of the temperature did not exceeded 2°C and that of the relative humidity did not exceed 5 %. In most of the cases the standard deviations were much more less than these values.

2
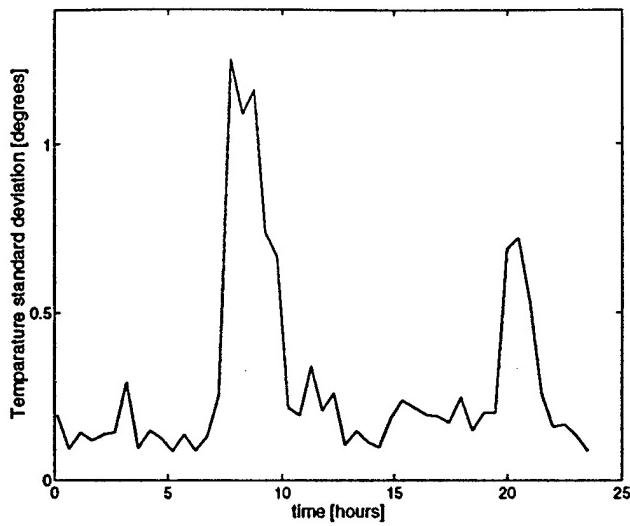
Fig. 1. Half hour standard deviation of air temperature as a function of time during a typical summer day.
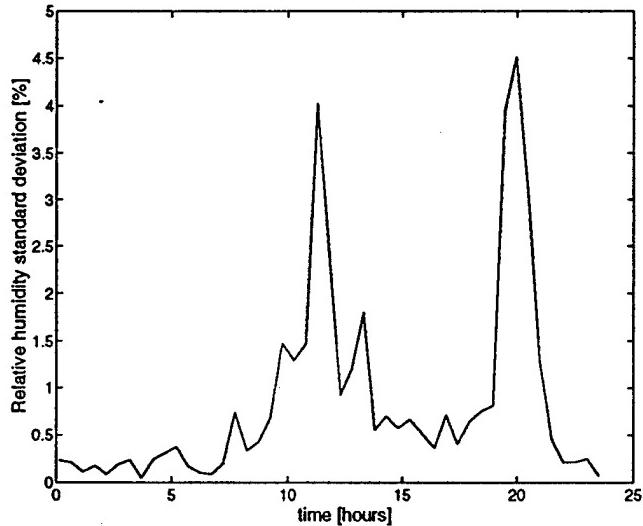

Fig. 2. Half hour standard deviation of relative humidity as a function of time during a typical summer day.

3. Data Analysis

The deviations in the aerosol size distribution are large. The aerosols in the area of our measurements consist of a large variety of aerosol sources. Aerosol chemistry and area meteorology are described in detail in ref. 2. The aerosol sources are urban and rural, marine, haze, industrial and desert dust aerosols that are transferred from the Sahara desert and from the Arabian desert[4] during dust storms,

3

Fig. 3. describes two extreme aerosol size distributions that were measured during the year 1992. The differences between the two extreme cases is about two orders of magnitude. The lower curve is not continuous because particles at several radii were not counted during an integration period of half an hour. Fig. 4. shows the normalized standard deviation of the measured aerosol at each radius. The standard deviation ranges from 0.5 at radius of 0.16 μm to 12 at radius of 10 μm. The aerosol size distribution consists of several distributions that can be modeled by superposition of lognormal distributions.[5] The standard deviation of the particle count is smaller for small radii than for high radii since the low, or fine mode of the aerosol distribution consists mainly of local aerosols while the large aerosol population contains also particles that are transported from remote areas. The local aerosols are less affected by changes in the weather parameters while the larger particles are very sensitive to the wind speed and to the wind direction which, in some cases, yields information concerning the source of the remote aerosols.

A simple size distribution that can characterize the coarse aerosol size distribution is the Junge power law distribution.[6] The size distribution is defined by only two parameters A and α:

$$\frac{dn}{dr} = Ar^{-\alpha} \tag{1}$$

r is the particle radius and n is the particulate number concentration.
The advantage of this size distribution is that a measured size distribution can be fitted to this model by a simple one variable linear regression.

In our analysis the measured size distributions were fitted to Junge power law models. The data were separated into two major groups. One consists of the measured data during the summer season from May to October. This corresponds to arid and semi-arid regions. The second group consisted of data that was measured during the winter season, starting from November until April. This corresponds to wet, non-arid regions.

The climate in our region is such that there are two major seasons. Summer is the hot and dry season with no participation at all. Winter is the colder season. All participation is during this season.

3.1 A model for the summer season

Fig. 5. describe the average particulate size distribution and the power law fit. All 6000 measurements of the aerosol size distribution from May 1992 to October 1992 were fitted to the power law distribution and the values of α and A were extracted. The average square of the correlation coefficient R^2 was 0.95.

The power law size distribution parameters A and α were related to the weather parameters that were measured nearby the particulate counter using multiple linear regression analysis. The summer model obtained for A is given by:

$$A = a_0 + a_1 rh + a_2 rh^2 + a_3 rh^3 + a_4 rh^4 \tag{2}$$

were rh is the relative humidity. The coefficient of the model are given in table 1.

4

Table 1. Summer model for the prediction of the parameter A.

a_0	a_1	a_2	a_3	a_4
1.917	-0.128	$4.61 \cdot 10^{-3}$	$6.85 \cdot 10^{-5}$	$3.73 \cdot 10^{-7}$

The model obtained for α was the following:

$$\alpha = b_0 + b_1\, rh + b_2\, rh + b_3\, ws \qquad (3)$$

were ws is the average wind speed in m/s. The coefficients for the prediction of α are given in table 2.

Table 2. Summer model for the prediction of the parameter α.

b_0	b_1	b_2	b_3
2.68	$2.3 \cdot 10^{-3}$	$8.16 \cdot 10^{-5}$	$-2.65 \cdot 10^{-2}$

The A parameter in this model depends only on the relative humidity. Other dependencies were weak and insignificant. The parameter α depends also on the average wind speed. Fig. 6 describes in an ascending order the measured α and the modeled α. From this figure it is shown that there is a good agreement between the measured parameter and the modeled parameter except for extreme weather conditions. Fig. 7. shows the measured parameter A in ascending order and the modeled parameter. The model gives good correlation here too except for extreme weather conditions.

Figs. 8. show typical measured particulate aerosol distributions (solid lines) and predicted size distribution according to the measured weather parameters (dashed lines). The curves shows that there is a very good agreement between the measured data and the model for the parameters α and A under a variety of weather conditions.
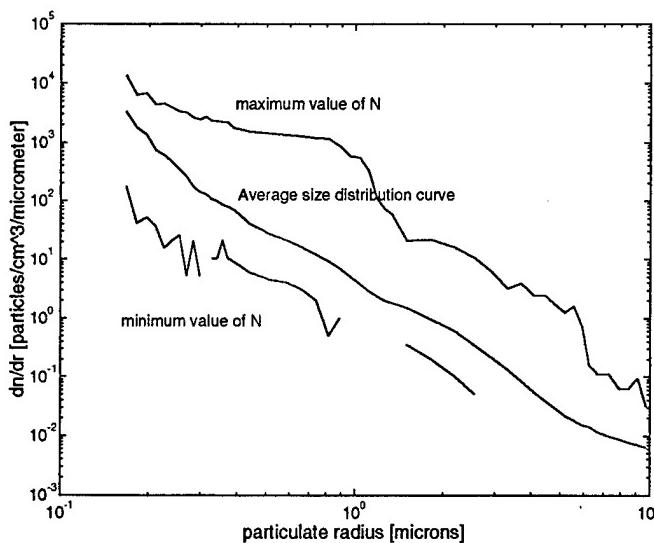

Fig. 3. Average aerosol size distribution curve and size distributions with the property of minimum and maximum number of particles that were measured.
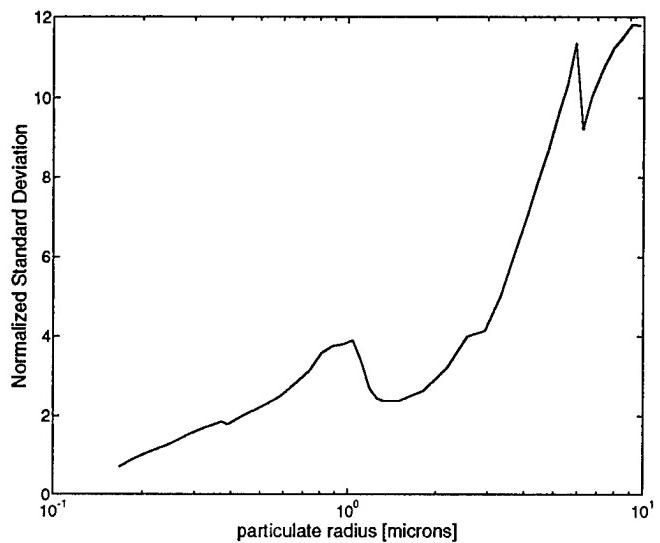
Fig. 4. Normalized standard deviation of the aerosol size distribution.
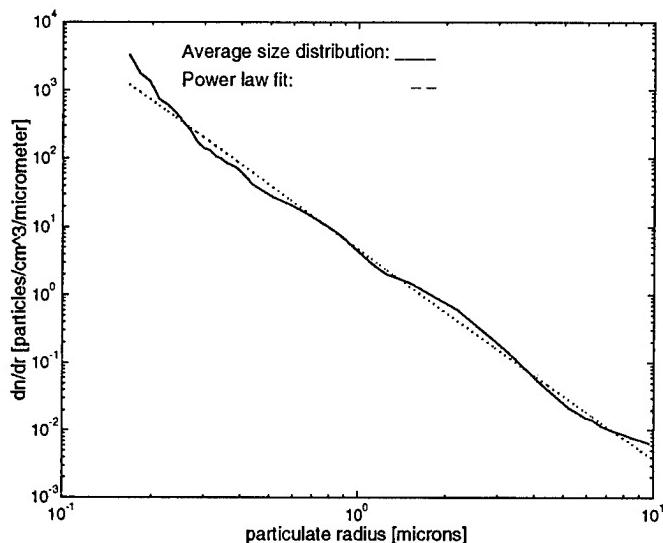
Fig. 5. The measured average particulate size distribution and its power law fit.
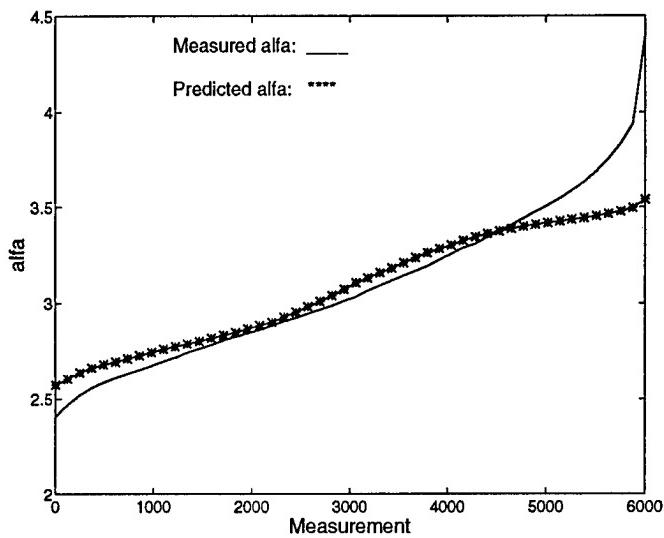
Fig. 6. Measured α parameter and predicted α.
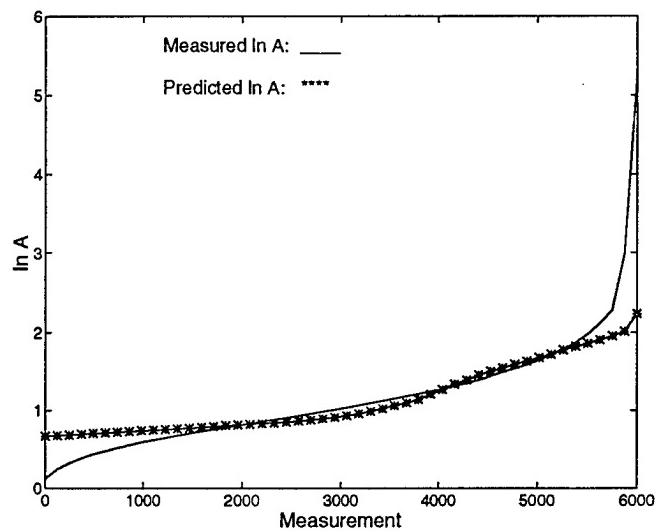
Fig. 7. Measured A parameter and predicted A.
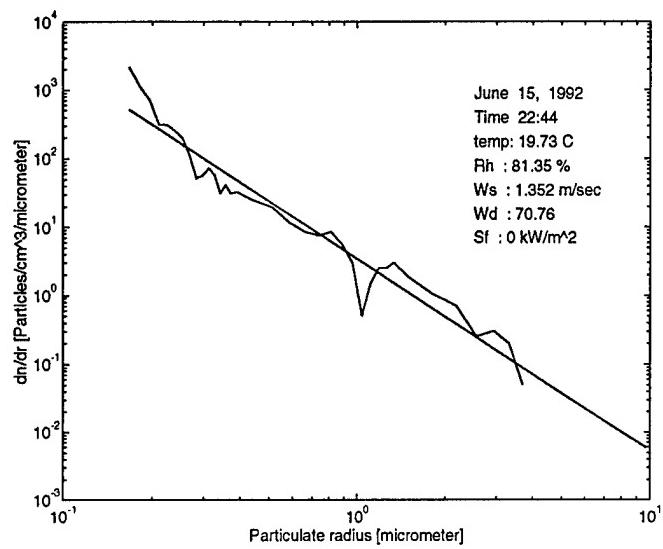
Fig. 8a. Measured particulate size distribution and the modeled size distribution.
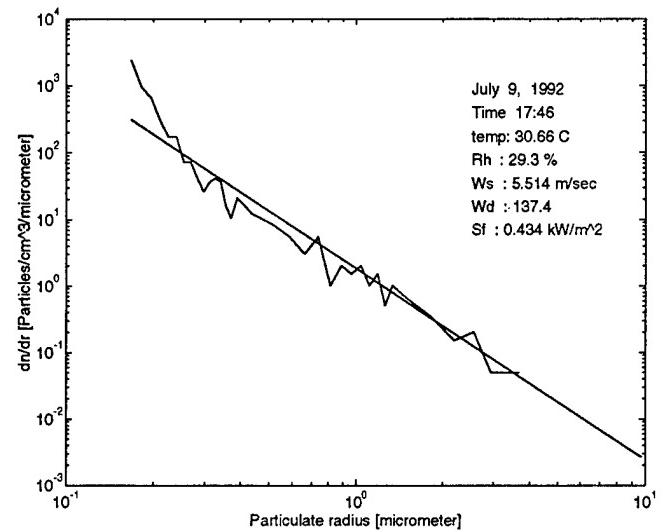

Fig. 8b. Measured particulate size distribution and the modeled size distribution.
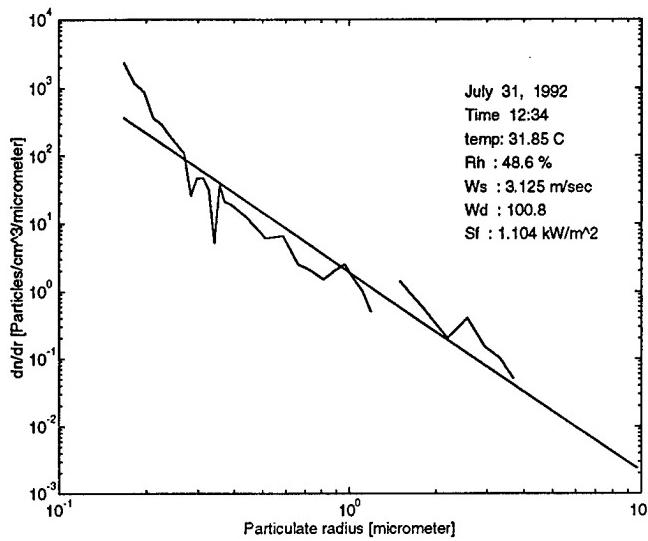
Fig. 8c. Measured particulate size distribution and the modeled size distribution.

4.2 A model for the winter season

A similar approach for modeling the aerosol size distribution for the winter season which is the wet and rainy season in our area was used. The two parameters of the power law model for the aerosol size distribution were related to weather parameters. The major difference between the two seasonal models is that for the winter season, not only were the measured weather parameters necessary but also the history of some of them. The model here is based on about 5000 different measurements of the aerosol size distribution during winter seasons.

The model for ln A is the following:

$$\ln A = a_0 + a_1\, rh + a_2\, \overline{rh}_{24} + a_3\, (\overline{rh}_{24})^2 + a_4\, ws + a_5\, \overline{ws}_{24} + a_6\, (\overline{ws}_{24})^2 + a_7\, tm + a_8\, sf \quad (4)$$

where rh is relative humidity, $\overline{rh}_{24}$ is the last 24 hour average of the relative humidity, ws is the wind speed in m·s^{-1} $\overline{ws}_{24}$ is the 24 average of the wind speed, tm is the temperature in ° C, and sf is the solar flux in kwatt·m^{-2}.

The following model was obtained for α:

$$\alpha = b_0 + b_1\, rh + b_2\, \overline{rh}_{24} + b_3\, (\overline{rh}_{24})^2 + b_4\, ws + b_5\, \overline{ws}_{24} + b_6\, (\overline{ws}_{24})^2 + b_7\, tm + b_8\, sf \quad (5)$$

Fig. 9 show an example of the measured aerosol size distribution and the modeled size distribution according to the weather parameters and the 24 hour averages of the wind speed and the relative humidity.
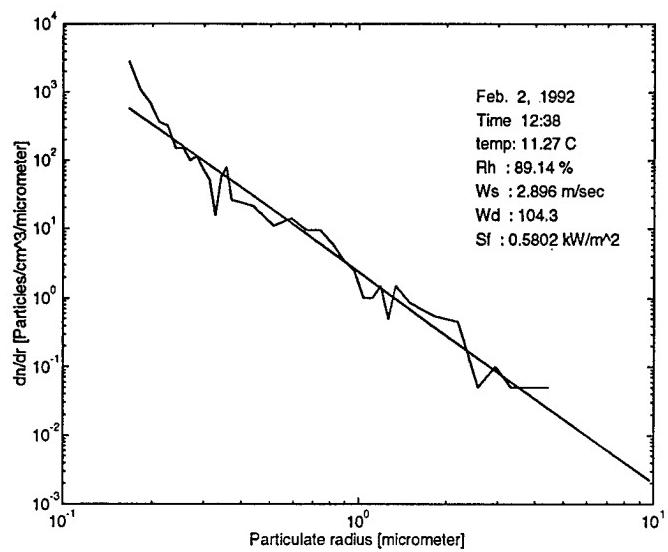
Fig. 9. Measured particulate size distribution and the modeled size distribution for the winter season.

5. Conclusions

The major conclusion of this research is that the coarse aerosol size distribution parameters can be predicted according to simple meteorological parameters. A strong statistical relation exists between the aerosol size distribution curve and the local weather. Although the Junge power law distribution is not accurate since it does not model the size distribution at radii that are smaller than 0.1 μm and the fine details of the curve are lost, it can model roughly the aerosol size distribution and it is very easy to extract its two parameters A and α even if the aerosol histogram is composed of relatively low counts of particles. The strong statistical dependence of the power law distribution on local weather parameters show us that in most cases the statistics of the aerosols are influenced by the local weather. There are few exceptions, mainly when the aerosol size distribution consists of particles such as desert dust particles or marine particles that are transported from other areas.

Introducing the history of the meteorological parameters such as the previous 24 hours average of the wind speed and that of the relative humidity was very significant to the winter model and contributed significantly to the correlation of the model with measurement.

6. References

1. I. Dror and N. S. Kopeika, "Aerosol and Turbulence MTFs: Comparison Measurements in the Open Atmosphere," *Optics Letters* 17, 1532-1534, 1992.
2. J. Gottlieb, B. Fogel, I. Dror, Z. Y. Offer, and N. S. Kopeika, "Prediction of airborne particle statistics according to weather forecast: concentration and scattering area," to be published in *Opt. Eng.*
3. I. Dror and N. S. Kopeika, "Prediction of aerosol distribution parameters according to weather forecast," in *Atmospheric Propagation and Remote Sensing*, A. Kohnle and W. Miller, eds., Proc SPIE, vol. 1688, 123-131, 1992.
4. E. Ganor, H. A. Foner, S. Brenner, E. Neeman, and H. Lavi, "The chemical composition of aerosols settling in Israel following dust storms," Atmosph Environment, 25A, No. 12, 2665-2670, 1991.
5. E. P. Shettle and R. W. Fenn, "Models for the aerosols of the lower atmosphere and the effects of humidity variations on their optical properties," AFGL-TR-79-0214, 1979.
6. M. M. R. Williams and S. K. Loyalka, *Aerosol Science*, Chap. 1, Pergamon Press, 1991.

Appendix 2

Calculating Practical Aerosol MTF

Mie scattering, absorption and extinction coefficients
Mie phase function

1. Define the following parameters

   m - relative refractive index (complex).
   λ - radiation wavelength (meters).
   a - particle radius (meters).
   $x = \dfrac{2\pi\, a}{\lambda}$ - size parameter.
   $\rho = x \cdot m$.
   θ - scattering angle (steradians).
   $\mu = \cos\theta$.
   $n(x)$ = particle size distribution

2. Create the *spherical Bessel functions*, which satisfy the recurrence relations

$$z_{n-1}(\rho) + z_{n+1}(\rho) = \frac{2n+1}{\rho} z_n(\rho), \tag{1}$$

$$(2n+1)\frac{d}{d\rho} z_n(\rho) = n\, z_{n-1}(\rho) - (n+1) z_{n+1}(\rho), \tag{2}$$

where z_n is either j_n or y_n. From the first two orders

$$j_0(\rho) = \frac{\sin\rho}{\rho}, \qquad\qquad j_1(\rho) = \frac{\sin\rho}{\rho^2} - \frac{\cos\rho}{\rho}, \tag{3}$$

$$y_0(\rho) = -\frac{\cos\rho}{\rho}, \qquad\qquad y_1(\rho) = -\frac{\cos\rho}{\rho^2} - \frac{\sin\rho}{\rho}, \tag{4}$$

higher-order functions can be generated by recurrence.

3. Create the *spherical Bessel functions of the third kind* (Hankel functions)

$$h_n(\rho) = j_n(\rho) - i\, y_n(\rho). \tag{5}$$

4. Create the *Riccati-Bessel functions*

$$\varphi_n(\rho) = \rho\, j_n(\rho), \qquad\qquad \xi_n(\rho) = \rho\, h_n(\rho). \qquad (6)$$

5. Calculate the *scattering parameters* a_n and b_n

$$a_n = \frac{m\varphi_n(\rho)\varphi_n'(x) - \varphi_n(x)\varphi_n'(\rho)}{m\varphi_n(\rho)\xi_n'(x) - \xi_n(x)\varphi_n'(\rho)}, \qquad (7)$$

$$b_n = \frac{\varphi_n(\rho)\varphi_n'(x) - m\varphi_n(x)\varphi_n'(\rho)}{\varphi_n(\rho)\xi_n'(x) - m\xi_n(x)\varphi_n'(\rho)}. \qquad (8)$$

6. Calculate the *Mie scattering, extinction and absorption efficiency factors*

$$Q_{sc}(m,x) = \frac{2}{x^2} \sum_{n=1}^{\infty} (2n+1)\left(|a_n|^2 + |b_n|^2\right), \qquad (9)$$

$$Q_{ext}(m,x) = \frac{2}{x^2} \sum_{n=1}^{\infty} (2n+1)\,\mathrm{Re}\{a_n + b_n\}, \qquad (10)$$

$$Q_{abs} = Q_{ext} - Q_{sc}. \qquad (11)$$

7. Create the *angle-dependent functions* which satisfy the recurrence relations

$$\pi_n = \frac{2n-1}{n-1}\mu\,\pi_{n-1} - \frac{n}{n-1}\pi_{n-2}, \qquad (12)$$

$$\tau_n = n\mu\,\pi_n - (n+1)\pi_{n-1}, \qquad (13)$$

where $\pi_0 = 0$ and $\pi_1 = 1$.

8. Calculate the *complex amplitudes* of scattered electric fields

$$S_1(m,x,\theta) = \sum_{n=1}^{\infty} \frac{2n+1}{n(n+1)}(a_n\pi_n + b_n\tau_n), \qquad (14)$$

$$S_2(m,x,\theta) = \sum_{n=1}^{\infty} \frac{2n+1}{n(n+1)}(b_n\pi_n + a_n\tau_n) \qquad (15)$$

where S_1 and S_2 are components perpendicular and parallel to the scatter plane.

9. Calculate the *dimensionless intensity parameters* (for scattered light only)

$$i_1(x,m,\theta) = S_1 S_1^*, \qquad (16)$$

$$i_2(x,m,\theta) = S_2 S_2^*. \qquad (17)$$

10. Use the *measured* atmospheric particle size distribution to calculate the *medium's scattering coefficient* (scattering cross section per unit volume)

$$S_a[\lambda, n(x)] = \pi k^{-3} \int_0^\infty x^2 n(x) Q_{sc}(x) dx. \tag{18}$$

11. Calculate the *medium's phase function*

$$P(\theta) = \frac{2\pi}{k^3 S_a} \int_0^\infty n(x)[i_1(\theta) + i_2(\theta)] dx, \tag{19}$$

which obeys the normalization condition:

$$\int_\Omega P(\theta) dw = 4\pi \tag{20}$$

where the integration is with respect to solid angle over all directions corresponding to all space around a point.

12. Calculate the *medium's extinction coefficient* (extinction cross section per unit volume)

$$\sigma[\lambda, n(x)] = \pi k^{-3} \int_0^\infty x^2 n(x) Q_{ext}(x) dx, \tag{21}$$

13. Calculate the *medium's absorption coefficient* (absorption cross section per unit volume)

$$A_a[\lambda, n(x)] = \pi k^{-3} \int_0^\infty x^2 n(x) Q_{abs}(x) dx, \tag{22}$$

Atmospheric absorption - spatial frequency dependence

14. Calculate aerosol MTF including absorption spatial frequency dependence

$$M_a(f_a) = \exp\left\{-S_a z \left(\frac{f_a}{f_{ac}}\right)^2\right\} \cdot \exp\left\{\left[\exp\left\{-S_a z \left(1 - \left(\frac{f_a}{f_{ac}}\right)^2\right)\right\} - \exp\{-S_a z\}\right](-A_a z)\right\}, \quad f_a < f_{ac}$$

$$\exp\{-S_a z\} \cdot \exp\{[1 - \exp\{-S_a z\}](-A_a z)\}, \qquad f_a > f_{ac}. \tag{23}$$

15. Calculate the new MTF asymptote at high spatial frequencies = $M_a(\infty)$ (differing from the atmospheric transmittance), and calculate the *effective optical depth*

$$T_{eff} = -\ln[M_a(\infty)]. \tag{24}$$

Practical aerosol MTF

16. Approximate the medium's phase function by a Gaussian form (not necessary)

$$P(\theta) = 4\sqrt{\pi \alpha_p} \exp\{-\alpha_p \theta^2\}. \tag{25}$$

17. Calculate the "classical" aerosol MTF using the *effective optical depth*

$$K(f_a) = \exp\left\{-\int_0^z T_{eff}\left[1 - \exp\left(-\frac{\pi^2 f_a^2}{\alpha_p}\right)\right]dz'\right\}. \tag{26}$$

18. Determine the main instrumentation limitations:
    a - Finite angular spatial frequency bandwidth - $f_a\max$.
    b - Finite field of view - Θ'_{max}.
    c - Dynamic range limitation - minimal detected received irradiance, which is related to maximal angle of *detected* scattered light - Θ''_{max}.
    d - SNR limitation - minimal detected received irradiance, which is of higher intensity than the background noise - Θ'''_{max}.

19. Choose the worst case between (18b) - (18d), obtaining the instrumentation limitation of maximal angle of recorded scattered light - $\Theta_{max} = \min\left\{\Theta'_{max}, \Theta''_{max}, \Theta'''_{max}\right\}$

20. Calculate the "classical" *specific intensity function* for the case of an infinite plane-wave

$$I(\theta) = \frac{1}{(2\pi)^2}\int_{-f_{a\,max}}^{f_{a\,max}} d f_a \cdot \exp(-j\theta f_a)\cdot K(f_a). \tag{27}$$

20a. In case where the system's MTF is known, (27) can be replaced by

$$I(\theta) = \frac{1}{(2\pi)^2}\int_{-\infty}^{\infty} d f_a \cdot \exp(-j\theta f_a)\cdot K(f_a)\cdot M_0(f_a) \tag{27a}$$

where $M_0(f_a)$ is the system MTF.

21. Calculate the *practical aerosol MTF* by inverse Fourier transforming the specific intensity function

$$PMTF_a(f_a) = \int_{-\Theta_{max}}^{\Theta_{max}} d\theta \cdot \exp(j\theta f_a)I(\theta). \tag{28}$$

Appendix 3

Comparison between high-resolution restoration techniques of atmospherically distorted images

D. Sadot, S. R. Rotman, and N. S. Kopeika

Department of Electrical and Computer Engineering

Ben-Gurion University of the Negev

Beer-Sheva, Israel

Abstract

A system approach is applied to overcome atmospheric degradation of remotely sensed images. A comparison is presented between different filtering techniques for restoration of distorted images for both the visible and thermal infrared spectral regions. Restoration methods include spatial and spatial frequency filters. Best results are obtained by using a fractal model to describe the image's power spectral density for scenes in the visible spectral range. Atmospheric effects are best modeled by a noisy spatial frequency filter composed of an average component described by the average atmospheric and hardware modulation transfer function, and a noisy component modeled by the atmospheric point spread function's power spectral density. The most impressive restorations in the visible range are achieved by combining between the last and the fractal model for the object's power spectral density. In the thermal range, however, several restoration techniques yielded very good results, with no one technique most advantageous over the others. The methods presented here are capable of yielding real-time image restoration with resolution limited essentially only by the hardware itself in both wavelength regions.

1. Introduction

Imaging through the atmosphere has progressed significantly in the last decade, in both the visible and infrared spectral ranges. It is the atmosphere which usually limits image quality, particularly for long atmospheric paths. The main atmospheric distortions are caused by optical turbulence, and scattering and absorption by particulates in the atmosphere. The main effect of the turbulent medium over long exposures is to produce wavefront tilt, which causes image shifts at the image plane. These can be whole image shifts, or different shifts of different parts of the image, depending on the isoplanatic patch, according to the turbulence parameters (turbulence strength, inner and outer scales). The image distortions caused by the wavefront tilt (typically on the order of tens or maybe hundreds of microradians) can be partially compensated for either by adaptive optics techniques or by using sufficiently short exposure time, less than the characteristic fluctuation time (usually a few milliseconds). Another way is by using a wavefront sensor to construct the image phase in addition to image intensity, and therefore restore the image in a deterministic way[1]. This is, however, not practical for real time restoration. Turbulence distortion effects are characterized in both short and long exposures by modulation transfer functions (MTFs)[2,3]. These are statistical averages of turbulence random processes which have, in addition, a nonnegligible short-time variance which affects significantly image blur. In addition to turbulence, there are scattering and absorption effects produced by molecules and aerosols in the atmosphere. These cause both attenuation and image blur, according to the atmospheric aerosol MTF[4-9]. Unlike turbulence, the aerosol MTF affecting the image is also related strongly to instrumentation limitations[6,8,9] on the angles of light scatter actually recorded in the image. Thus, aerosol effects can be approximated by an MTF of limited long-time variation, according to weather conditions.

Here, image processing techniques are aided by the knowledge of the corruption from which the image has suffered while propagating through the atmosphere. These techniques are preferable rather than standard blind-deconvolution techniques, as long as the corrupting medium, i.e. atmosphere, is modeled sufficiently accurately. One way of modeling the

atmospheric distortions is by the average atmospheric MTF. In this technique, atmospheric effects are modeled by a deterministic filter. This method yields good restoration results when atmospheric MTF does not vary too much, particularly when turbulence effects are not dominant. This is the case in the thermal range, or while only low spatial frequencies are involved. When turbulence is dominant, however, modeling atmospheric MTF by a deterministic filter is insufficient, due to significant MTF variance. Atmospheric effects in that case should be modeled by a *noisy* spatial frequency filter including an average component described by the average atmospheric MTF, and a noisy component which contains the MTF variance.

The power spectral density (PSD) of the original picture is often required in order to apply the restoration filter to the corrupted image (as in the standard Wiener filter, for example). One way of estimating this term is by rigorously assuming that it equals the image's PSD. This is of course not true, but in many cases this is a sufficiently good assumption. To check this issue, one can restore the image iteratively. This process should stop when restored images converge. Usually, it happens after one or two iterations. Another way of estimating the object's PSD is by assuming it obeys a fractal model. It will be shown here that using a fractal estimation model yields very good results for visual images.

In this paper, the fractal dimension estimation process is presented, Then, the improved Wiener filter technique is introduced. This is followed with other spatial filtering restoration techniques. Results of the different methods will be compared, including some examples of restored thermal images as well as visible images.

2. Fractal model

If it were possible to know characteristics of the original background with which one was dealing, one could potentially design more efficient and effective algorithms to perform the restoration. In this paper, we describe the restoration of images for natural scenes. It has been proposed that natural scenes are fractal in nature; pictures taken in the visual spectral range

will also be fractal[10] (in contrast to infrared images which tend to be modeled by Markov random fields[11].

Our restoration of the scenes based on their similarity to fractal models is performed as follows[12]. Fractal scenes in the visual regime have power spectra with a $\frac{1}{f^n}$ frequency dependence. We assume that even in real natural pictures, the $\frac{1}{f^n}$ behavior will be correct for wide bands of frequencies. The types of blurring which occur will affect the higher frequencies much more than the lower frequencies. We rather arbitrarily assume that the corruption has only occurred to the highest frequencies for which 0.1% of the energy of the picture is found; although this seems minuscule, in a large number of picture distortions this is indeed where the major changes occur. The remaining power of the lower frequencies are fit to $\frac{1}{f^n}$ where n is determined by a least-square fit of the log of the radial power to the frequency. We then assume that the higher frequencies in the original picture originally followed the same $\frac{1}{f^n}$ dependence before corruption. These frequencies are then restored.

Results of images restored by using best fits between the object's PSD to fractal model are presented in Fig. 1. It is clear that scene's resolution is improved. This method yields very good results for pictures which include relatively "natural" scenes. However, when the scenes become more "man-made", restoration efficiency decreases. In the thermal range, however, the fractal model completely failed, as demonstrated in Fig. 2. Both "man-made"[12] and thermal images[11] are known not to be fractal in nature, but rather Markovian; thus failure of a fractal method is not unexpected.

3. Improved Wiener filter

The improved Wiener filter[13] is based on the standard Wiener filter[14], with an additional noise model deriving from the atmospheric MTF variance. As explained in the introduction, the atmospheric MTF derives from both turbulence and aerosol forward scattering effects. While aerosol MTF is fairly constant as long as atmospheric conditions do

not vary too much, turbulence MTF changes with time due to it's tilt jitter characteristic. These tilts are random and their temporal power spectra are usually limited to several tens up to a few hundred hertz under ordinary atmospheric conditions. The image distortions caused by atmospheric MTF are thus regarded as the sum of a deterministic and a random filter[15,16]. The deterministic filter includes aerosol[6,9] and average turbulence MTFs[2-5], while the random filter includes the noise component induced on the imaging system, both by the turbulence MTF variance and hardware[13]. Stated mathematically, the atmospheric filter is determined by

$$h' = h + n_1 \tag{1}$$

where h' is the instantaneous atmospheric point spread function (PSF), h is the average atmospheric PSF, and n_1 is an additive random component with zero expectation. Using this model, the image received at the imaging system after propagating through the atmosphere is:

$$g(x,y) = \big(h(x,y) + n_1(x,y)\big) \otimes f(x,y) + n_2(x,y) \tag{2}$$

where g is the received image, f is the object, x and y are transverse spatial coordinates, and n_2 is an additive noise imposed by the instrumentation, including optics, digitization, electronics etc., but not by the atmosphere. Fourier transforming (2) yields:

$$G(u,v) = [H(u,v) + N_1(u,v)] \cdot F(u,v) + N_2(u,v) \tag{3}$$

where G, H, F, N_1 and N_2 are Fourier transforms of g, h, f, n_1 and n_2 respectively, and u and v are spatial frequency coordinates. The received image thus is a sum of a deterministic part G_1 and a random part N

$$G = G_1 + N \tag{4}$$

where
$$G_1(u,v) = H(u,v) \cdot F(u,v) \tag{5}$$

and
$$N(u,v) = F(u,v) \cdot N_1(u,v) + N_2(u,v). \tag{6}$$

The improved Wiener filter is defined similarly to the standard Wiener filter, differing by the noise component which includes an additional term imposed by the atmosphere[13]

$$M(u,v) = \frac{|H(u,v)^2|}{H(u,v) \cdot \left(|H(u,v)^2| + \left[S_{n_1 n_1}(u,v) + S_{n_2 n_2}(u,v) / S_{ff}(u,v) \right] \right)} \tag{7}$$

where M is the restoring filter, $H(u,v)$ is the average atmospheric MTF, $S_{n_1 n_1}(u,v)$, $S_{n_2 n_2}(u,v)$, and $S_{ff}(u,v)$ are the power spectral densities of f, n_1, and n_2, where n_1 and n_2 are the inverse Fourier transforms of N_1 and N_2 in (6).

Assuming independence between aerosol and turbulence effects, the term $H(u,v)$ can be measured or calculated by a multiplication of the turbulence MTF (either short or long exposure case) and aerosol MTF. Turbulence MTF can be evaluated with the knowledge of standard meteorological parameters using a C_n^2 prediction model[17] (verified independently by U.S. Army Night Vision Laboratory) or IMTURB or PROTURB (U.S. Army Atmospheric Sciences Lab.), and the aerosol MTF[6] can be evaluated according to knowledge of particle size distribution, which can also be predicted via LOWTRAN, MODTRAN, or other models[18]. The term $S_{ff}(u,v)$ can be estimated either by using the received image $G(u,v)$ or by using estimation models of the object's PSD, which has been shown to obey a fractal model in the visible range, and a Markovian model in the thermal range[11]. The term $S_{n_2 n_2}(u,v)$ is assumed to be constant for all spatial frequencies since the additive noise n_2 is assumed to be white noise. This assumption is commonly used and very practical, and it has a relatively weak effect on the Wiener filter. The term $S_{n_1 n_1}(u,v)$ is very important, since it includes the random part of the atmospheric distortions. One way of estimating $S_{n_1 n_1}(u,v)$ is by a direct measurement. By using the relation

$$S_{n_1 n_1}(u,v) = E\{N_1^2(u,v)\}, \tag{8}$$

and the Fourier transform of (1), i.e.,

$$N_1(u,v) = H'(u,v) - H(u,v), \tag{9}$$

it follows that $S_{n_1 n_1}$ equals the variance of the instantaneous atmospheric MTF:

$$S_{n_1 n_1}(u,v) = E\{H'^2(u,v)\} - H^2(u,v). \tag{10}$$

Since the contribution to the random part of the atmospheric MTF is due mainly to turbulence rather than aerosols, in (8)-(10) atmospheric MTF refers to turbulence only. However, in (7), $H(u,v)$ includes aerosol MTF in addition to turbulence MTF since it refers to the average atmospheric MTF. The variance of H' can be evaluated by calculating both terms of the right hand side of (8). This can be carried out by measuring a series of instantaneous atmospheric

MTFs, and evaluating the average of both the MTF and its square. This is, however, not a very practical way, particularly when *real time* image restoration is concerned.

An alternative way of obtaining $S_{n_1 n_1}(u,v)$ is by evaluating both terms of the right hand side of (10). The second term H^2 is the square of the turbulence MTF which can be predicted[17] or measured. The first term $E\{H'^2\}$ was evaluated analytically[13] and yields:

$$E\{H'^2(u,v)\} \propto H^2(u,v)\iint_\infty H^2(u',v')H(u'+u,v'+v)H(u'-u,v'-v)du'dv'. \quad (11)$$

Equation (11) determines the expected value of the squared MTF, or in other words the Point Spread Function's Power Spectral Density. The integral in (11) can be evaluated numerically with the use of the average turbulence MTF only.

Examples of restored images using this technique, obtained over a 6.5 km horizontal path length through the atmosphere, are presented in Fig. 3. The restoration was carried out by the use of (7). The term $H(u,v)$ was the measured atmospheric MTF. The term $S_{ff}(u,v)$ was estimated by best fit to a fractal model. Obtaining the term $S_{ff}(u,v)$ from the received image iteratevely yielded less impressive results. The term $S_{n_2 n_2}(u,v)$ was assumed to be white noise and the term $S_{n_1 n_1}(u,v)$ was evaluated via (11). Restoration time was only about 2 seconds per frame. This can be shortened to a fraction of a second, using parallel processing techniques already available. Therefore restoration via this method can be in real time. There is a distinct improvement in fine details of the images, even though the image's SNR is not degraded significantly. This is so in spite of the severe imaging conditions (long horizontal distance), where turbulence isoplanatic patch was less than image size, and standard Wiener filters failed completely in trying to restore the image, as can be seen in Fig. 4. In the standard Wiener filter, $S_{nn}(u,v)$ refers to white noise only.

The improved Wiener technique yielded very good results in the thermal range too (8-12 μm spectral window), and restoration[9] for a picture obtained over a 2 km horizontal path length through the atmosphere, using this technique, are presented in Fig. 5. The term $S_{ff}(u,v)$ was estimated from the received image, and no iteration was needed (restoration converged after the first iteration). Since the thermal images involved significantly lower resolution than those in the visible range (due to instrumentation limitations), the main atmospheric distortions were due to aerosol rather than turbulence MTF. Therefore, as

explained previously, MTF variance was significantly weaker and restoration was possible using an average atmospheric MTF (rather than instantaneous), as demonstrated at the bottom right of Fig. 5. This is important while considering real time restoration since atmospheric MTF can be estimated once to create an efficient restoration filter which can be used for a large set of images. The fact that atmospheric MTF in the thermal range is relatively static causes relatively impressive restoration results using standard Wiener filters (which failed in the visible range). An example can be seen in Fig. 6.

4. Constrained filter

The constrained filter[14] uses a prior knowledge about the picture corruption i.e. atmospheric distortions, in addition to many kinds of constraining conditions, in order to achieve best restoration performance. The constraining conditions can also depend upon prior knowledge about the target. In that case, improved restoration results are expected, but the filter must be adapted to the kind of scene which is to be restored. Here, a more general condition is used, which is restoration using the atmospheric MTF, under the condition of maximal smoothness. This condition minimizes noise effects due to the high frequency enhancement which overcome MTF degradation. The smoothness, however, causes limited performance on sharp edges restorations.

We assume that $H(u,v)$ is the average atmospheric MTF, the original picture is of dimensions MxN, and the MTF and PSF are of dimensions JxK. Each matrix is padded with zeros to obtain $(M+2J)x(N+2K)$ matrix size. A two dimensional second order derivation is defined by the Laplacian matrix

$$[l] = \begin{bmatrix} 0 & 1 & 0 \\ 1 & -4 & 1 \\ 0 & 1 & 0 \end{bmatrix}. \tag{12}$$

The mathematical form of the constrained filter is given by:[14]

$$M(u,v) = \frac{1}{H(u,v)} \cdot \frac{|H(u,v)^2|}{(M+2J)(N+2K)\left(|H(u,v)^2| + \frac{1}{\lambda}|L(u,v)|^2\right)} \tag{13}$$

where $L(u,v)$ is the Fourier transform of $[l]$, and λ is obtained by Lagrange multipliers technique, or can be evaluated iteratively. An example of image restoration, obtained over a 6.5 km horizontal path length through the atmosphere, using the constrained filter is presented in Fig. 7. It is clear that in the restored image additional details are resolvable which can not be seen in the original picture, such as the two horizontal bars at the bottom of the picture.

5. Modified Backus-Gilbert filter

The modified Backus-Gilbert filter[19] is a spatial domain filter. It is assumed that the atmospheric point spread function is a finite impulse response (FIR), and so is the restoring filter. Here, in the examples to be shown it is assumed that the PSF's dimensions are 15x15 pixels. Two criteria in the restored image are implemented. These are image sharpness, in order to resolve details as fine as possible, and minimum noise variance. Image sharpness is obtained by narrowing the restored PSF as much as possible.

Defining the atmospheric PSF as $h(x,y)$ and the restoring filter as $m(x,y)$, the restored PSF is defined as

$$\hat{h}(x,y) = h(x,y) \otimes m(x,y). \tag{14}$$

In order to achieve perfect restoration, $\hat{h}(x,y)$ should be as close to an impulse as possible. One possible measure of a narrow restored PSF is a minimized second moment, i.e.

$$R = E\left\{\int r^2 \hat{h}(x,y)dxdy\right\} \to \min \tag{15}$$

where $r^2 = x^2 + y^2$ represents the coast of spread of $\hat{h}(x,y)$.

The requirement of minimizing noise variance can be stated mathematically as:

$$V = E\left\{\hat{n}^2(x,y)\right\} \to \min \tag{16}$$

where

$$\hat{n}(x,y) = n(x,y) \otimes m(x,y) \tag{17}$$

is the noise of the restored image.

Since minimizing average spread R and minimizing noise variance V can not be achieved simultaneously, a tradeoff between resolution and noise must be accomplished, and a compromise is by minimizing the weighted sum:

$$F = (1-\lambda)R + \lambda V \to \min, \tag{18}$$

where λ should be selected according to the restoration requirements, blur versus noise. A detailed mathematical description of solving (18) is presented in Ref. 19.

An example of image restoration, for the same scene as in Fig. 3, using the modified Backus-Gilbert filter, is presented in Fig. 8. Another example is in the thermal range, where this filter yielded very good restoration results. This is demonstrated in Fig. 9 for the same scene as in Fig. 5.

6. Discussion

A comparison between the different restoration techniques indicates that the filter of best performance is the improved Wiener filter. This is explained by the use of the atmospheric model as a noisy filter, due to turbulence jitter characteristics. Thus, when dealing with high resolution visible and near infrared imaging through long distances, atmospheric distortions need no longer be treated as a deterministic filter represented by average MTF, but can now be modeled as an inherent part of the noise in the received image. Determining this random part is essential to achieving improved restored images, and a method of doing so is presented here. This method can be used to help overcome the jitter characteristic of turbulence, and is capable of real time image restoration via parallel processing transputers. As turbulence effects becomes weaker, such as in the thermal image example, the advantage of this method diminishes, and standard Wiener filter performance is fairly good. The original picture's power spectral density, for visible images, is best estimated using a fractal model. This model yielded very good results using both the fractal estimation filter and the improved Wiener filter. This model failed completely when used to restore thermal images. It is expected that, due to energy transfer considerations, thermal images will obey instead a Markovian power spectral density model. Thermal images restoration thus is a subject for further investigation, using the

Markovian model. In cases where a smooth image, rather than a sharp but noisy one is required, the constrained filter can be used to satisfy this condition. This is also the case when using the modified Backus-Gilbert filter, which has also the advantage of shorter computation time. In any case where turbulence is not too dominant, the last two filters yield impressive results (as in the thermal range). However, as atmospheric MTF variance increases, it is strongly recommended to use the improved wiener filter, which indeed yielded the best results.

Conclusions

Restorations of visible and thermal images distorted by the atmosphere are presented based upon atmospheric MTF. Such restoration techniques are fundamental and include both spatial and spatial frequency filters. In the restored images it is generally quite possible to see detail almost as small as possibly resolvable by instrumentation, i.e. pixel size. In the visible image examples, pixel size at 6.5 km horizontal distance is ~7 cm. Examples for finest resolvable details are poles in a fence and antenna bars(~ 7 cm). In the thermal images, pixel size at 2 km is ~62 cm, and examples of finest resolvable details are windows whose size is about the same. This means that, essentially, all atmospheric blur is removed in the restoration process, and the distant object scene is observed as if there were no atmosphere. This can only be possible by considering the atmospheric MTF properly, including the significant role played by aerosol MTF. Such restoration does not depend on target shape. It is a fundamental image correction, which can be followed by other image processing techniques as required. In the visible range an improved Wiener filter designed specifically for imaging through the atmosphere, together with a fractal estimation model for the object's power spectral density, appears to give excellent results. In the thermal infrared, where turbulence effect is less severe, several different filters each give excellent results. There are cases where turbulence is not so severe, and aerosol MTF plays the most important role in determining the atmospheric MTF, such as in the case of thermal imaging, and the image restoration task is much easier since the atmospheric MTF then is nearly deterministic. Here, however, the correction is for both aerosol and turbulence derived blur.

Acknowledgment

References

1. J. Primot, G. Rousset and J. C. Fontanella, Deconvolution from wavefront sensing: a new technique for compensating turbulence-degraded image," *J. Opt. Soc. of Amer. A,* **7**, No. 9, pp. 1598-1608, September 1990.

2. D. Fried "Optical resolution through a randomly inhomogeneous medium for very long and very short exposure," *J. Opt. Soc. of Amer.* **56**, No. 10, 1372-1379, October 1966.

3. J. W. Goodman, *Statistical Optics*, John Wiley & sons, New York, 1985.

4. A. Ishimaru, *Wave propagation and scattering in random media,* Volume 1, Academic Press, New York, 1978.

5. R. F. Lutomirski "Atmospheric degradation of electrooptical system performance," *Applied Optics*, **17**, No. 24, pp. 3915-3921, December, 1978.

6. D. Sadot and N. S. Kopeika, "Practical instrumentation-based theory and verification of aerosol MTF," *J. Opt. Soc. of Amer. A,* **10**, No. 1, pp. 172-179, January 1993.

7. I. Dror and N. S. Kopeika, "aerosol and turbulence MTFs: comparison measurements in the open atmosphere," Opt. Lett. **17**, No. 22, pp. 1532-1534, 15 Nov. 1992.

8. D. Sadot and N. S. Kopeika "Thermal imaging through the atmosphere: Atmospheric MTF theory and verification," to be published in *Optical Engineering,* **33**, March 1994.

9. D. Sadot, A. Dvir, I. Bergel and N. S. Kopeika, "Restoration of thermal images distorted by the atmosphere, based upon measured and theoretical atmospheric modulation transfer function," to be published in *Optical Engineering*, **33**, January 1994 (special issue on Infrared Technology).

10. A. P. Pentland, "Fractal based description of natural scenes, " IEEE Trans. Patt. Anal. & Machine Intelligence, **6**, 661-674, 1989.

11. G. Tidhar, S. R. Rotman, and M. L. Kowalczyk," Clutter matrics for target detection systems," IEEE Trans. on Aerospace and Electr. Syst., Jan 1994 (in press).

12. G. Cohen, G. Reina, G. Tidhar, and S. R. Rotman, "Improved electro-optical target detection in a natural fractal enviroment," in *8th meeting on Optical Engineering and Remote Sensing*, Moshe Oron, Itzhak Shladov, and Yitzhak Weissman, editors, Proc. SPIE, Vol. 1971, 78-92, 1993.

13. D. Sadot, A. Rosenfeld, G. Shuker, and N. S. Kopeika, "High resolution restoration of images distorted by the atmosphere, based upon average atmospheric MTF," submitted for publication.

14. A. Rosenfeld, and A. C. Kak, *Digital picture processing*, Academic Press, London, 1976.

15. L. Guan and R. K. Ward, "Restoration of randomly blurred images by the Wiener filter," IEEE, *Trans. on Acoustics, Speech, and Signal Processing*, **12**, No. 4, pp. 589-592, April 1989.

16. L. Guan and R. K. Ward, "Deblurring random time-varying blur," *J. Opt. Soc. of Amer. A,* **6**, No. 11, pp. 1727-1737, November 1989.

17. D. Sadot and N. S. Kopeika, "Forecasting optical turbulence strength on the basis of macroscale meteorology and aerosols: models and validation," *Optical Engineering* **31**, No. 2, pp. 202-212, February, 1991.

18. I. Dror and N. S. Kopeika, "Prediction of particulate size distribution according to weather parameters," in *Atmospheric Propagation and Remote sensing*, A. Khonle and W. B. Miller eds., Proc. SPIE, Vol. 1668, pp. 123-131, 1992.

19. R. K. Ward and B. E. A. Saleh, "Deblurring random blur," IEEE Transactions on Acoustics, Speech, and Signal Processing, **ASSP-35**, No. 10, October 1987.

Figure captions

Fig. 1.　Restoration of two scenes at 6.5 km horizontal distance (visible wavelengths) using fractal PSD best fit.

Fig. 2.　Restoration of a thermal (8-12 μm) image of a scene at 2 km horizontal distance using fractal PSD best fit.

Fig. 3.　Improved Wiener filter restoration, using fractal PSD estimation of scenes of Fig. 1.

Fig. 4.　Standard Wiener filter restorations of scenes of Fig. 1.

Fig. 5.　Improved Wiener filter restoration of a thermal (8-12 μm) image at 2 km horizontal distance.

Fig. 6.　Standard Wiener filter restoration of the thermal image of Fig. 5.

Fig. 7.　Restoration of scene at 6.5 km horizontal distance (visible wavelengths) using constrained filter.

Fig. 8.　Restoration using modified Backus-Gilbert filter of scene of Fig. 3.

Fig. 9.　Restoration of a thermal image using modified Backus Gilbert FIR filter (same scene as Figs. 5 and 6).

original picture

original picture

fractal estimation
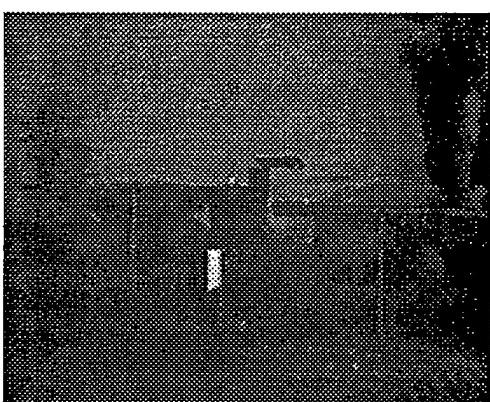
fractal estimation
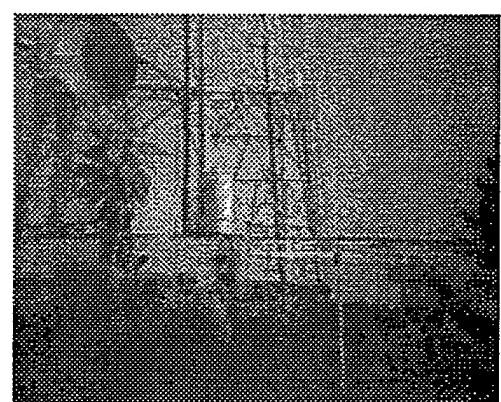
Fig 1

original picture
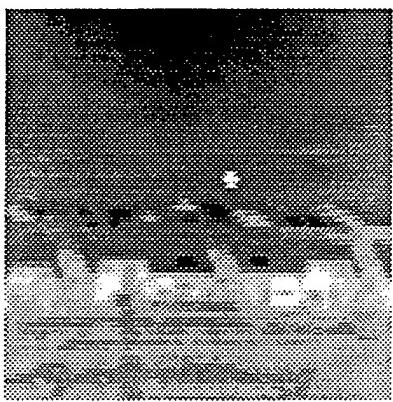
fractal estimation

Fig 2

original picture
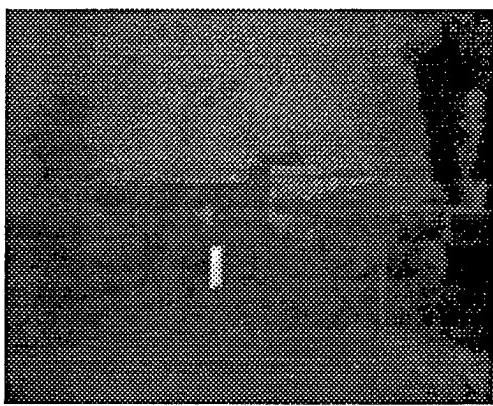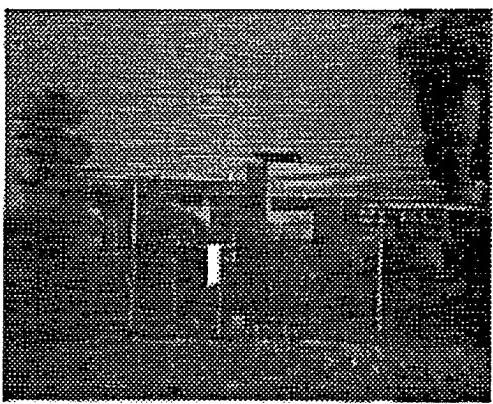
original picture

restoration with improved Wiener

restoration with improved Wiener

Fig 3
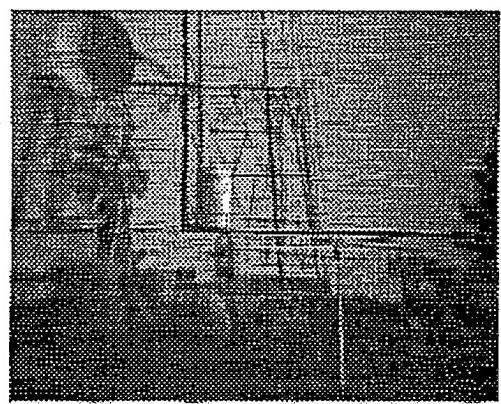
original picture

original picture

restoration with standard Wiener

restoration with standard Wiener
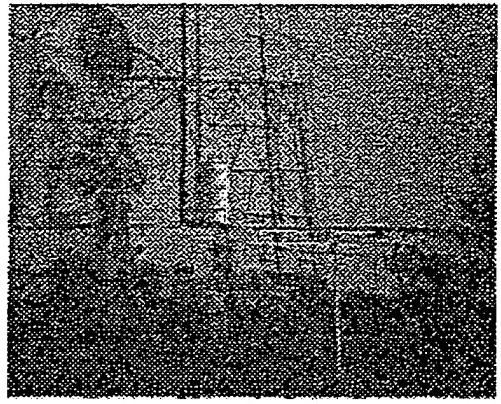
Fig 4

original picture

restoration with improved Wiener

restoration with average MTF

Fig 5
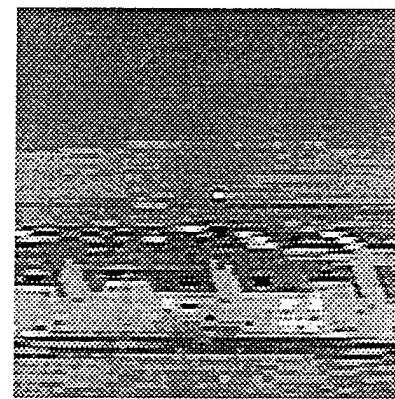
original picture

restoration with wiener filter

restoration with average MTF

Fig 6
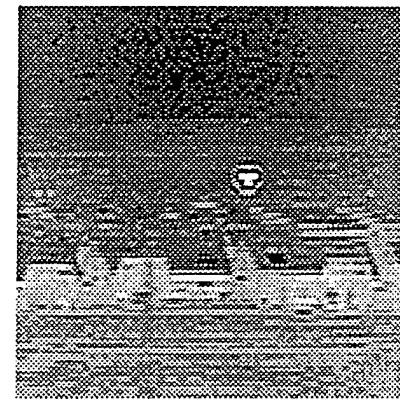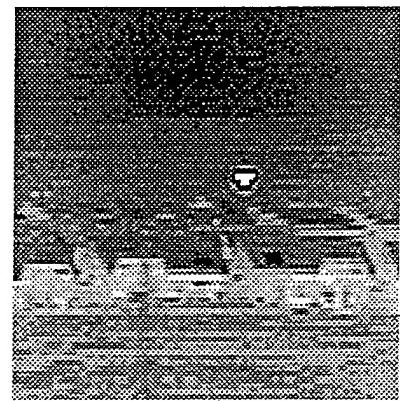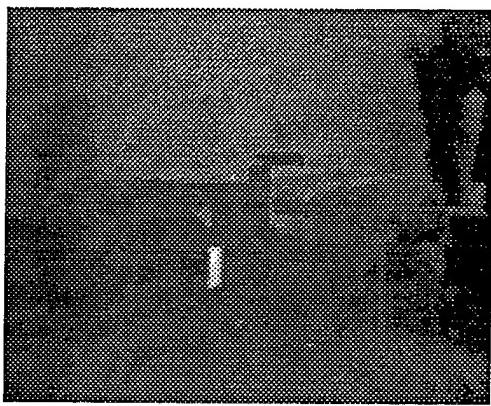
original picture
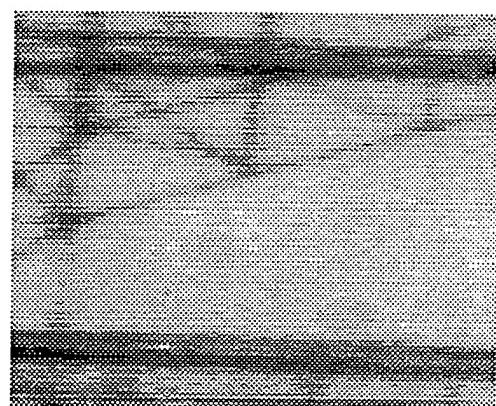
original picture

restoration with Backus-Gilbert
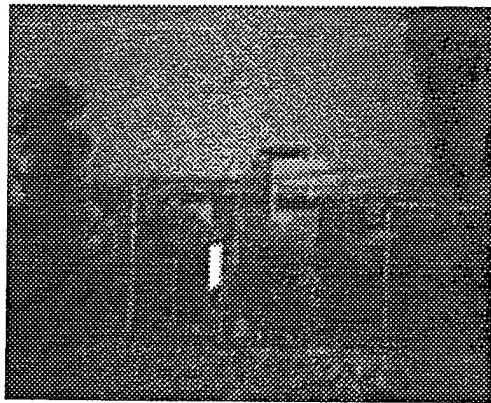

restoration with constrained filter
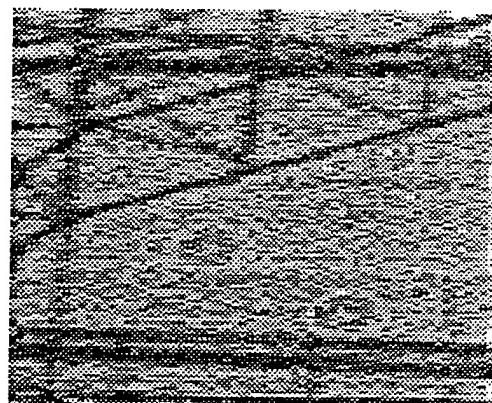
Fig 8

Fig 7

original picture
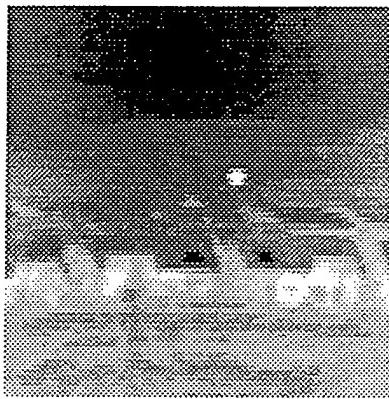
restoration with FIR filter

restoration with average MTF

Fig. 9